The $[Fe(etz)_6](BF_4)_2$ Spin-Crossover System—Part One: High-Spin $\rightleftharpoons$ Low-Spin Transition in Two Lattice Sites

Roland Hinek, Hartmut Spiering, Dieter Schollmeyer, Philipp Gütlich* and Andreas Hauser*

Dedicated to Professor Hans Georg von Schnering on the occasion of his 65th birthday

Abstract: The $[Fe(etz)_6](BF_4)_2$ spin-crossover system (etz = 1-ethyl-1*H*-tetrazole) crystallizes in space group $P\bar{1}$, with the following lattice constants at 298 K: a = 10.419(3), b = 15.709(1), c = 18.890(2) Å; α = 71.223(9), β = 77.986(10), and γ = 84.62(1)°; V = 2862.0(9) Å^3 and Z = 3. Two nonequivalent lattice sites, one without (site A) and one with (site B) inversion symmetry, are observed. The population of the two sites n_A:n_B is 2:1. Iron(II) on site A undergoes a thermal low-spin (LS) $\rightleftharpoons$ high-spin (HS) transition with $T_{1/2}$ = 105 K, whereas that on site B remains in the high-spin state down to cryogenic temperatures. Application of external pressure of up to 1200 bar between 200 and 60 K does not cause formation of the low-spin state on site B. On site A the high-spin state can be populated as a metastable state at 20 K by irradiating the sample with λ = 514.5 nm; on site B a light-induced population of the low-spin state can be achieved with λ = 820 nm.

Keywords
iron complexes · LIESST · spin crossover · tetrazoles

1. Introduction

Spin crossover has been a well-known phenomenon in first-row transition metal chemistry for some decades. It has been reviewed by many authors primarily for iron(II) complexes.[1, 2, 3, 4] The compounds $[Fe(Rtz)_6](BF_4)_2$ (Rtz = 1-alkyl-1*H*-tetrazole) belong to the large group of octahedrally coordinated iron(II) spin-crossover compounds exhibiting an entropy-driven spin transition from the $^1A_1$ low-spin (LS) ground state at low temperatures to the $^5T_2$ high-spin (HS) state at elevated temperatures. The series with R = $-CH_3$, $-CH_2CH_3$ and $-CH_2CH_2CH_3$ provides an example of the strong interdependence between crystal structure and spin-transition features, which both vary drastically with the substituent R of the monodentate ligands. For instance, in the monoclinic methyl derivative $[Fe(mtz)_6](BF_4)_2$ (space group $P2_1/n$, Z = 4),[5] the iron(II) complexes occupy two nonequivalent lattice sites (sites A and B) to equal extents. The complexes on site A show a steep thermal spin transition at $T_{1/2}$ = 75 K. The transition temperature is defined as the temperature at which the HS fraction γ_{HS} is equal to 0.5. In contrast, the complexes on site B remain in the HS state down to 10 K.[6] On the other hand, in the rhombohedral propyl derivative $[Fe(ptz)_6](BF_4)_2$ (space group $R\bar{3}$, Z = 3) at 297 K,[5] all complexes are equivalent. Here, a quantitative thermal spin transition with hysteresis takes place ($T_c^{\downarrow} \approx 128$ K, $T_c^{\uparrow} \approx 135$ K). The hysteresis is due to a first-order crystallographic phase transition from the rhombohedral high-temperature phase ($R\bar{3}$) to the triclinic low-temperature phase ($P\bar{1}$).[5, 7] The spin transition itself is quantitative within the two structural phases.

In $[Fe(ptz)_6](BF_4)_2$ the HS state can be populated as a metastable state well below the thermal transition temperature by irradiating at the spin-allowed $^1A_1 - {}^1T_1$ d–d absorption band.[8, 9] The mechanism for this process, known as light-induced excited spin state trapping (LIESST),[10] is shown in Figure 1. Owing to the large energy barrier between the HS and LS states resulting from the difference in metal–ligand bond length of approximately 0.2 Å, the lifetime of the light-induced HS state at 20 K is over 10 days.[11] Only at T > 50 K does a noticeable HS → LS relaxation set in. The metastable HS state can also be depopulated at 20 K by irradiation into the $^5T_2 - {}^5E$ band (reverse-LIESST).[12] The depopulation is not quite quantitative because of the spectral overlap of the $^5T_2 - {}^5E$ band and the spin-forbidden transitions of the LS species. This results in a steady-state type situation with a residual HS fraction of around 10%.[10]

In the methyl derivative $[Fe(mtz)_6](BF_4)_2$, the complexes on lattice site A behave in much the same way as in $[Fe(ptz)_6](BF_4)_2$; those on lattice site B can only be converted to the LS state as a metastable state by irradiation with λ = 820 nm.[6, 13]

[*] A. Hauser
Institut für Anorganische, Analytische und Physikalische Chemie
Universität Bern, Freiestrasse 3, CH-3000 Bern (Switzerland)
Fax: Int. code +(31)65-3993
e-mail: ahauser@iac.unibe.ch

P. Gütlich, R. Hinek, H. Spiering
Institut für Anorganische Chemie und Analytische Chemie
Universität Mainz, Staudingerweg 9, D-55099 Mainz (Germany)
Fax: Int. code +(6131)39-2990
e-mail: guetlich@dacmza.chemie.uni-mainz.de

D. Schollmeyer
Institut für Organische Chemie der Universität Mainz
Becherweg 18-20, D-55099 Mainz (Germany)
Fax: Int. code +(6131)39-4778
e-mail: scholli@uacdr0.uni-mainz.de

  0947-6539/96/0211-1427 $ 15.00+.25/0

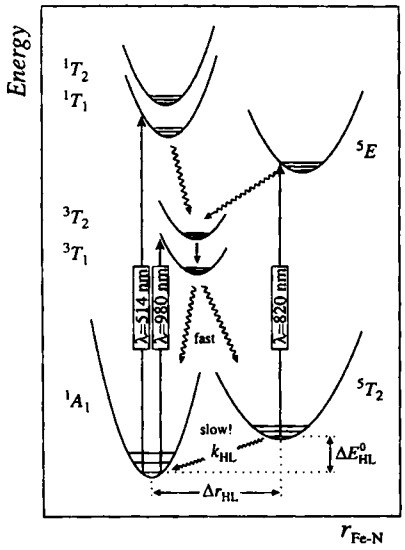

Fig. 1. Schematic potential surfaces of the low-lying ligand-field states for a d^6 spin-crossover compound. The arrows at $\lambda = 514$ and 820 nm indicate the LIESST and reverse-LIESST effects, respectively. LIESST is also observed by irradiation into the triplet bands at $\lambda = 980$ nm [10].

In continuation of our studies on iron(II) spin-crossover compounds belonging to the tetrazole class, our interest has focussed on the $[Fe(etz)_6](BF_4)_2$ system, that is, the ethyl derivative within the alkyl homologuous series $[Fe(Rtz)_6](BF_4)_2$. The basic results of this investigation are presented in this paper, including the crystal structure of $[Fe(etz)_6](BF_4)_2$, which provides the basis for understanding the thermal and light-induced spin-transition behaviour of this system.

Table 1. Crystallographic data and structure refinement for $[Fe(etz)_6](BF_4)_2$ [a].

empirical formula	$C_{18}H_{36}N_{24}B_2F_8Fe$
formular weight	818.11
crystal size/mm	$0.52 \times 0.44 \times 0.16$
absorp. coeff./mm^{-1} (no corr.)	0.48
ρ_{calcd}/gcm^{-3}	1.424
crystal system	triclinic
space group	$P\bar{1}$
a/Å	10.419(3)
b/Å	15.709(1)
c/Å	18.890(2)
α/°	71.223(9)
β/°	77.986(10)
γ/°	84.62(1)
V/Å^3	2862.0(9)
Z	3
$F(000)$	1254
T	298
index ranges	$0 \le h \le 14$ $-21 \le k \le 22$ $-25 \le l \le 26$
diffractometer	Enraf-Nonius CAD-4
λ/Å	0.71070 ($Mo_{K\alpha}$)
monochromator	graphite
scan mode	$\omega/2\theta$
scan width/°	$\omega = 0.7 + 0.5\tan(\theta)$
θ range/°	1.5–30.0
reflections measured	17513
unique reflections	16669
refinement method	full-matrix least-squares on F^2
R_{int}	0.019
observed reflections	6779 ($\|F\|/\sigma(F) > 4.0$)
parameters	749
R indices	$R_1 = 0.103$, $wR_2 = 0.373$
max. shift/esd	0.01
largest diff. peak and hole/e Å^{-3}	1.05, −0.66

[a] Three standard reflections after 4000 s; fading of 30% compensated with spline approximation.

2. Results

2.1. Crystal Structure: $[Fe(etz)_6](BF_4)_2$ crystallizes in the triclinic space group $P\bar{1}$, $Z = 3$ (Table 1). Figure 2 shows the projection of the triclinic unit cell along the [1 0 0] axis. Two complexes

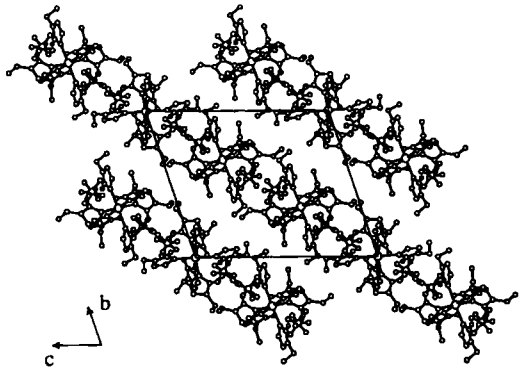

Fig. 2. Projection of the unit cell of $[Fe(etz)_6](BF_4)_2$ along the [1 0 0] axis. There are complex layers within the (0 1 −1) lattice planes. The stacking period of the layers is two. The distance between layers is ca. 11 Å, which is comparable to the corresponding distances in the methyl (≈8 Å) and propyl (≈11 Å) systems [5].

are located in general positions in the middle of the cell. They are connected by the central inversion symmetry and thus become symmetry equivalent. Furthermore, complexes in specific positions on the corners of the cell all show an inversion centre in $P\bar{1}$. Hence, these complexes themselves show inversion symmetry and constitute the third complex within the unit cell. The two nonequivalent lattice sites are henceforth denoted as site A (without inversion symmetry) and site B (with inversion symmetry). The population of the two sites $n_A:n_B$ is 2:1.

The complexes are stacked within electrically neutral layers parallel to the (0 1 −1) lattice planes. There is a cleavage plane parallel to these layers and a pseudotrigonal symmetry axis perpendicular to each layer, as visualized by Figure 3. The trigonal symmetry of the complex layers is also present in the crystal

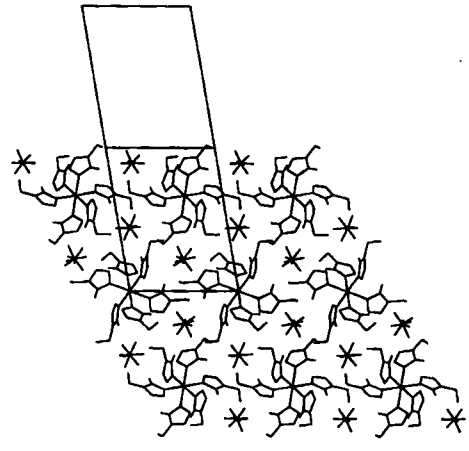

Fig. 3. Projection of the unit cell perpendicular to the (0 1 −1) lattice plane. There is a pseudotrigonal symmetry axis perpendicular to the complex layers.

0947-6539/96/0211-1428 $ 15.00+.25/0 Chem. Eur. J. 1996, 2, No. 11

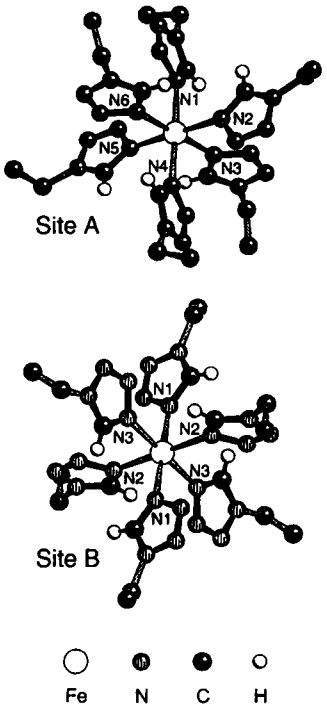

Fig. 4. Molecular structures of the $[Fe(etz)_6]^{2+}$ groups on site A and site B. For clarity only the aromatic H atoms are drawn.

structures of the mtz and ptz systems. It seems to be a general feature within the $[Fe(Rtz)_6](BF_4)_2$ series.[5]

At 298 K the BF_4^- groups are strongly disordered, giving rise to a rather poor R value of 0.103. Unfortunately, a structure determination at 100 K failed because the crystal quality worsened rapidly during the measurement. The molecular structures of the A- and B-site complex cations are shown in Figure 4, with the labelling of all nitrogen atoms that participate in the metal–ligand bonds of the complexes. The iron–nitrogen bond lengths are listed in Table 2. The octahedral environment is nearly perfect for the two sites.

Table 2. Iron–nitrogen bond lengths (Å) at the two sites in $[Fe(etz)_6](BF_4)_2$.

Site A		Site B	
Fe–N1	2.180(4)	Fe–N1	2.203(4)
Fe–N2	2.182(5)	Fe–N2	2.190(5)
Fe–N3	2.182(5)	Fe–N3	2.196(4)
Fe–N4	2.187(4)		
Fe–N5	2.185(5)		
Fe–N6	2.183(4)		

2.2. Thermal Spin-Crossover

2.2.1. ^{57}Fe Mössbauer Spectroscopy under Normal Conditions: The ^{57}Fe Mössbauer spectrum at 295 K (Fig. 5) consists of two quadrupole doublets, typical for iron(II) in the HS state, with nearly the same isomer shifts and slightly different quadrupole splittings. The intensity ratio of the two HS doublets is 2:1, according to the unequal population of the two lattice sites. Hence, the less intense outer doublet can unambiguously be assigned to the complexes on site B [HS(B)], whereas the more intense inner doublet has to be identified as the resonance from site A complexes [HS(A)]. At 200 K the two doublets become much more readily discernible, because of the stronger temperature dependence of the quadrupole splitting for the HS(B) doublet. The difference in intensity between the two lines of a given doublet is due to texture caused by the flat pseudohexagonal crystals. At 120 K a new singlet appears in the spectrum with typical parameters for iron(II) in the LS state. The intensity of this singlet increases on lowering the temperature from 120 K (11%) down to 20 K (58%), mainly at the cost of the HS(A) intensity, which itself drops from 54 to 12%. Simultaneously there is a slight decrease of the HS(B) intensity from 35% at 120 K to 31% at 20 K. We conclude that the singlet mainly arises from complexes on site A. Thus, only site A complexes undergo a thermal spin transition, whereas complexes on site B

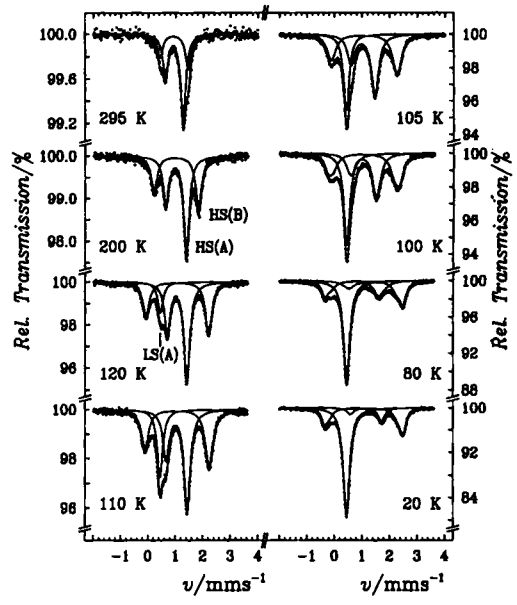

Fig. 5. ^{57}Fe Mössbauer spectra of $[Fe(etz)_6](BF_4)_2$ recorded at various temperatures under normal pressure.

do not show a thermal spin transition or, if at all, only to a small extent. The site A spin transition is not quite quantitative, because of a residual HS(A) intensity in the spectrum at 20 K (Fig. 5). Thus the overall HS fraction of 42% at 20 K is composed of HS(B) (31%) and HS(A) (11%) complexes.

The fraction of the HS(A) resonance of the total intensity as a function of temperature gives the thermal spin transition curve with a transition temperature $T_{1/2} = 105$ K (Fig. 6). The temperature dependence of the quadrupole splittings ΔE_Q of the HS(A) and HS(B) doublets is very different. ΔE_Q of HS(A) is nearly temperature independent, whereas ΔE_Q of HS(B) varies strongly with temperature. A similar behaviour was also found in the $[Fe(mtz)_6](BF_4)_2$ system and has been discussed by Poganiuch et al.[6] A characteristic feature of $[Fe(etz)_6](BF_4)_2$ is the line broadening of the Mössbauer lines, especially of the HS doublets, upon decreasing the temperature to below 105 K. The full half-width $\Gamma_{HS(B)}$ of the HS(B) lines increases from 0.22 mm s^{-1} at 295 K to 0.38 mm s^{-1} at 105 K. Upon further cooling the lineshapes become very complicated. In order to evaluate at least the relative intensities of the HS and LS species from the broadened spectra, the spectra recorded below 105 K were fitted with two doublets of Lorentzian lineshape for each of the HS(A) and the HS(B) resonances having the same isomer shifts and fixed textures, but with variable half-widths and quadrupole splittings. The Mössbauer parameters at 1 bar and for temperatures between 20 and 295 K are collected in Table 3a.

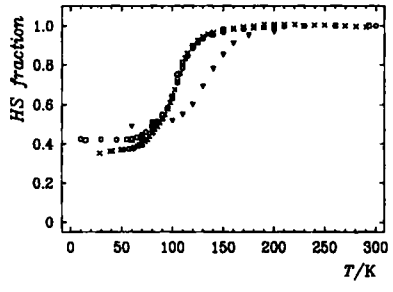

Fig. 6. Overall HS fraction γ_{HS} as a function of temperature in $[Fe(etz)_6](BF_4)_2$: at 1 bar from Mössbauer spectra (□), from magnetic susceptibility (×) and from optical absorption spectra (○); at 1200 bar from Mössbauer spectra (▽).

Table 3. ^{57}Fe Mössbauer parameters of the thermal spin transition in $[Fe(etz)_6](BF_4)_2$ [a].
a) Normal pressure (1 bar).

	HS(A)				HS(B)				LS			
T [K]	ΔE_Q [mm s^{-1}]	δ_{iso} [mm s^{-1}]	$\Gamma_{1/2}$ [mm s^{-1}]	γ_{HS}	ΔE_Q [mm s^{-1}]	δ_{iso} [mm s^{-1}]	$\Gamma_{1/2}$ [mm s^{-1}]	γ_{HS}	ΔE_Q [mm s^{-1}]	δ_{iso} [mm s^{-1}]	$\Gamma_{1/2}$ [mm s^{-1}]	γ_{LS}
295	0.65(2)	0.935(4)	0.116(8)	0.69	1.03(3)	0.924(8)	0.11(2)	0.31	–	–	–	–
200	0.751(5)	1.000*	0.118(3)	0.61	1.162(7)	1.006(4)	0.133(6)	0.39	–	–	–	–
150	0.746(4)	1.029(2)	0.121(2)	0.61	2.026(6)	1.035(3)	0.127(4)	0.37	–	0.43*	0.12(3)	0.03
120	0.721(4)	1.042(2)	0.130(2)	0.54	2.287(6)	1.051(3)	0.144(4)	0.35	–	0.430(5)	0.120(7)	0.11
110	0.776(5)	1.042(2)	0.138(2)	0.46	2.347(6)	1.056(3)	0.166(5)	0.35	–	0.433(3)	0.122(4)	0.19
105	0.87(1)	1.033(6)	0.159(5)	0.40	2.40(1)	1.083(7)	0.19(1)	0.35	–	0.426(3)	0.125*	0.25
100	0.82(2)/1.03(3)	1.041(4)	0.13(2)/0.12*	0.30	2.28(7)/2.62(4)	1.059(4)	0.16(1)/0.20(2)	0.34	–	0.436(1)	0.13(3)	0.35
80	1.03(7)/1.37(3)	1.06(1)	0.14(1)/0.18(3)	0.19	2.39*/2.85*	1.065(3)	0.25*/0.19*	0.30	–	0.440(1)	0.132(5)	0.51
70	0.97(8)/1.15(6)	1.08*	0.13(3)/0.135*	0.12	2.41(7)/2.86(2)	1.090(8)	0.14(4)/0.18(4)	0.31	–	0.427(2)	0.135*	0.56
60	1.03*/1.18*	1.088(5)	0.14*/0.14*	0.12	2.48*/2.90*	1.071(3)	0.14*/0.17*	0.30	–	0.441(1)	0.131(5)	0.59
20	1.13(2)/1.14(4)	1.14(1)	0.14*/0.14*	0.12	2.56(7)/2.88(2)	1.075(4)	0.16(2)/0.18(2)	0.31	–	0.440(1)	0.11(2)	0.58

b) External pressure of 1200 bar.

	HS(A)				HS(B)				LS			
T [K]	ΔE_Q [mm s^{-1}]	δ_{iso} [mm s^{-1}]	$\Gamma_{1/2}$ [mm s^{-1}]	γ_{HS}	ΔE_Q [mm s^{-1}]	δ_{iso} [mm s^{-1}]	$\Gamma_{1/2}$ [mm s^{-1}]	γ_{HS}	ΔE_Q [mm s^{-1}]	δ_{iso} [mm s^{-1}]	$\Gamma_{1/2}$ [mm s^{-1}]	γ_{LS}
200	0.708(5)	0.997(2)	0.12*	0.60	2.019(8)	1.016(4)	0.13*	0.37	–	0.44*	0.12*	0.02
175	0.713(5)	1.013(3)	0.13*	0.58	2.249(6)	1.028(3)	0.13*	0.37	–	0.44*	0.12*	0.05
160	0.723(5)	1.020(3)	0.13*	0.54	2.354(6)	1.035(3)	0.14*	0.37	–	0.438(8)	0.13*	0.09
150	0.755(5)	1.027(3)	0.132(3)	0.48	2.469(6)	1.041(3)	0.140(4)	0.37	–	0.438(4)	0.13*	0.15
140	0.811(6)	1.027(3)	0.139(3)	0.42	2.551(6)	1.044(3)	0.143(4)	0.36	–	0.435(3)	0.124(4)	0.22
130	0.88(1)	1.034(5)	0.153(4)	0.33	2.625(6)	1.045(3)	0.147(4)	0.36	–	0.436(2)	0.126(3)	0.31
120	0.98(2)	1.04(1)	0.17(1)	0.24	2.708(7)	1.051(4)	0.149(5)	0.36	–	0.435(2)	0.135(4)	0.40
110	0.85(1)	1.035(5)	0.141(5)	0.20	2.759(4)	1.050(2)	0.133(3)	0.35	–	0.436(1)	0.142(2)	0.45
100	0.83(1)	1.036(5)	0.128(7)	0.17	2.790(5)	1.053(2)	0.136(4)	0.36	–	0.438(1)	0.143(2)	0.48
80	0.83(1)	1.043(5)	0.113(5)	0.14	2.811(4)	1.062(2)	0.142(3)	0.37	–	0.440(1)	0.145(2)	0.49
60	0.84(1)	1.035(5)	0.111(6)	0.13	2.825(4)	1.065(2)	0.140(2)	0.37	–	0.442(1)	0.151(2)	0.51

[a] Spectra under 1 bar were measured in two series with different polycrystalline absorbers. Those under 1200 bar were recorded on a single crystal with a γ-ray direction perpendicular to the cleavage plane of the pseudohexagonal crystal, namely, the (0 1 −1) lattice plane. The asymmetric intensity ratio between the left and right lines of the HS doublets is taken from the 200 K spectrum at 1 bar and accepted for all other thermal spectra: $1/r = 1/2$ for HS(A) and 4/5 for HS(B). All spectra measured in cooling mode. The double-valued parameters ΔE_Q and $\Gamma_{1/2}$ of the HS species in Table 3a at temperatures below 105 K are due to the line broadening in this region (see text). Asterisks denote fixed parameters.

2.2.2. Magnetic Susceptibility: Figure 7 shows the effective magnetic moment of $[Fe(etz)_6](BF_4)_2$ calculated from the susceptibilities measured with a FONER magnetometer. The moment of 5.6 μ_B at 295 K is considerably larger than the spin-only moment of 4.9 μ_B, because of an orbital moment contribution due to the nearly ideal octahedral symmetry of the molecules. The moment drops to 3.45 μ_B at 60 K, as expected, since only around 60% of the complexes undergo a transition. The corresponding transition curve is included in Figure 6. Although quite steep, there is no hysteresis and the transition temperature $T_{1/2}$ of 105 K agrees well with the value from Mössbauer spectroscopy. The seemingly lower residual HS fraction at low temperatures is due to the deviation from the Curie law for Fe^{II} in almost perfectly octahedral coordination.

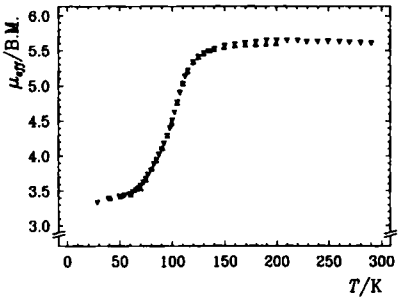

Fig. 7. Effective magnetic moment of $[Fe(etz)_6](BF_4)_2$ as a function of temperature in cooling mode (▽) and heating mode (△).

2.2.3. Optical Spectroscopy: Optical absorption spectra of $[Fe(etz)_6](BF_4)_2$ were measured between 300 and 10 K with a single crystal (Fig. 8). The spectrum at 300 K consists only of the $^5T_2 - {}^5E$ d–d band of the HS state centred at around 12000 cm^{-1}. The band is rather broad and it is not possible to distinguish between the lattice sites A and B. Upon cooling to below 170 K the $^1A_1 - {}^1T_1$ and the $^1A_1 - {}^1T_2$ d–d bands of the LS state begin to appear at approximately 18000 and 26000 cm^{-1}, respectively. On lowering the temperature down to 10 K the intensities of the singlet bands increase at the cost of the quintet intensity, owing to the spin transition on site A. The residual $^5T_2 - {}^5E$ intensity at 10 K mainly stems from HS(B) complexes on site B. $10Dq_{HS(B)}$ can be approximated from the maximum of the $^5T_2 - {}^5E$ band at 10 K to be 12070 cm^{-1}. $10Dq_{LS(A)}$ for the

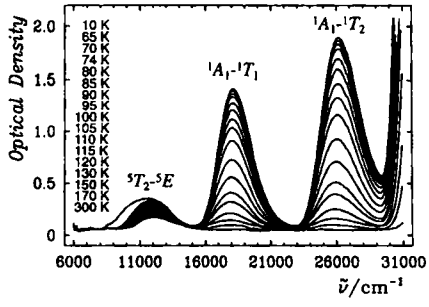

Fig. 8. Unpolarized single-crystal absorption spectra of $[Fe(etz)_6](BF_4)_2$ within the UV/Vis/NIR region at various temperatures. The band at 12000 cm^{-1} originates from the $^5T_2 - {}^5E$ transitions of the HS(A) and HS(B) complexes. The bands at 18000 and 26000 cm^{-1} arise from the $^1A_1 - {}^1T_1$ and the $^1A_1 - {}^1T_2$ transitions of the LS(A) complexes only.

0947-6539/96/0211-1430 $ 15.00+.25/0 Chem. Eur. J. 1996, 2, No. 11

LS(A) state can be estimated by using expression (1).[14] From

$$10Dq_{LS} = E(^1T_1) + \frac{E(^1T_2) - E(^1T_1)}{4} = 20120\ cm^{-1} \quad (1)$$

the normalized temperature-dependent $^1A_1 - {}^1T_1$ intensities the spin transition curve included in Figure 6 was obtained with $T_{1/2} = 105$ K. The normalization was performed by taking a HS fraction of 1.0 at 295 K and of 0.42 at 10 K, according to the relative intensities in the Mössbauer spectra at these temperatures.

2.2.4. ^{57}Fe Mössbauer Spectroscopy under Application of External Pressure: In order to try to convert the HS(B) state into its LS(B) state, external pressure and low temperatures were applied. The resulting ^{57}Fe Mössbauer spectra are shown in Figure 9. The spectra at 200 K under 1200 bar (Fig. 9) and 1 bar

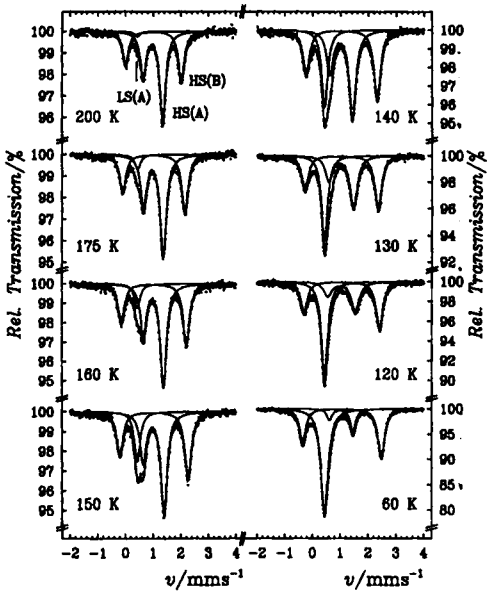

Fig. 9. ^{57}Fe Mössbauer spectra of $[Fe(etz)_6](BF_4)_2$ recorded at decreasing temperatures under an applied external pressure of 1200 bar. No formation of LS(B) is observed between 200 and 60 K.

(Fig. 5) look very similar. The additional appearance of a small LS(A) intensity under 1200 bar is not surprising at all, because the external pressure stabilizes the LS state. As a consequence, the site A spin transition is shifted from $T_{1/2} = 105$ K under normal conditions (Fig. 6) to $T_{1/2} \approx 140$ K under 1200 bar. However, application of pressure did not cause any LS formation on site B, since the full HS(B) intensity (≈37%) is present in the spectrum at 60 K under 1200 bar (Fig. 9). Furthermore, there is an evident line sharpening effect, as can be seen from Figure 10. The shoulder of the HS(B) resonance has vanished and also the linewidth of the HS(A) resonance has become smaller at 1200 bar compared to the spectrum under 1 bar. The Mössbauer parameters at 1200 bar are collected in Table 3b.

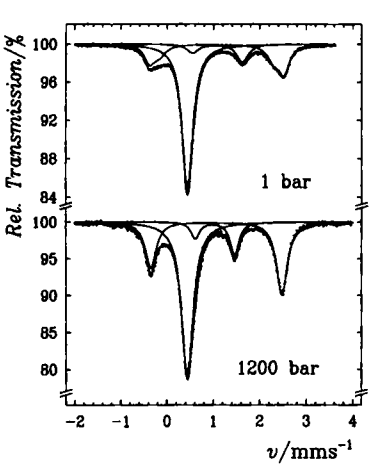

Fig. 10. ^{57}Fe Mössbauer spectra of $[Fe(etz)_6](BF_4)_2$ at 1 and 1200 bar both at 60 K. The linewidths at 1200 bar are much smaller than at 1 bar.

2.3. Light-Induced Spin-Crossover: In Figure 11 the light-induced spin transition processes of the complexes on the two lattices sites of $[Fe(etz)_6](BF_4)_2$ are documented by means of Mössbauer spectroscopy. Figure 11a shows the equilibrium spectrum at 20 K and Figure 11b the spectrum after irradiation with $\lambda = 514.5$ nm, that is, into the $^1A_1 - {}^1T_1$ band of the LS(A) complexes. After the irradiation the LS singlet disappeared completely; this indicates a quantitative light-induced LS(A) → HS(A) conversion, in analogy to the other Rtz systems.[6, 10] Irradiation with 820 nm, that is, into the $^5T_2 - {}^5E$ band of the HS(B) complexes, on the other hand, yielded the spectrum shown in Figure 11c, in which the HS(B) doublet has vanished. In contrast to other Rtz systems, where irradiation at 820 nm results in a steady state with approximately 85% LS caused by spectral overlap of the $^5T_2 - {}^5E$ band with spin-forbidden singlet–triplet bands, there is a quantitative HS(B) → LS(B) conversion, and only site A shows the expected behaviour with a residual HS fraction. The much less selective broad-band irradiation with $\lambda > 780$ nm, on the other hand, results in a steady-state behaviour on both sites. The corresponding spectrum shown in Figure 11d is conspicious for its substantially larger linewidths. Mössbauer parameters are collected in Table 4.

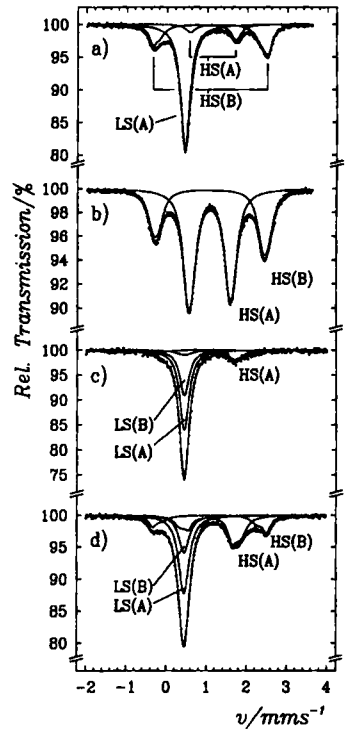

Fig. 11. ^{57}Fe Mössbauer spectra of $[Fe(etz)_6](BF_4)_2$ documenting the light-induced spin crossover processes on the two sites at 20 K: a) before irradiation, b) after irradiation with $\lambda = 514.5$ nm showing a quantitative LS(A) → HS(A) conversion, c) after irradiation with $\lambda = 820$ nm showing a quantitative HS(B) → LS(B) conversion, and d) after broad-band irradiation with $\lambda > 780$ nm showing partial HS(B) → LS(B) and LS(A) → HS(A) conversions.

Figure 12 shows the light-induced spin transitions by means of optical spectroscopy. With the results of Mössbauer spectroscopy we are able to interpret the spin conversions on the two sites. The loss of the whole singlet intensity in spectrum b is due to the quantitative population of the HS state on site A. In contrast, the increase in singlet intensity in spectrum c compared to that in spectrum a indicates the full HS → LS conversion on site B. At first sight the spectra a and d look rather similar, owing to comparable overall singlet intensities before (a) and after (d) broad-band irradiation. Nevertheless, the Mössbauer results should be born in mind, which revealed substantial spin conversions on the two sites after broad-band irradiation in Figure 11d.

Table 4. ^{57}Fe Mössbauer parameters after light-induced spin-crossover in $[Fe(etz)_6](BF_4)_2$ at 20 K [a].

	HS(A)				HS(B)				LS(A)				LS(B)			
	ΔE_Q [mm s^{-1}]	δ_{iso} [mm s^{-1}]	$\Gamma_{1/2}$ [mm s^{-1}]	γ_{HS}	ΔE_Q [mm s^{-1}]	δ_{iso} [mm s^{-1}]	$\Gamma_{1/2}$ [mm s^{-1}]	γ_{HS}	ΔE_Q [mm s^{-1}]	δ_{iso} [mm s^{-1}]	$\Gamma_{1/2}$ [mm s^{-1}]	γ_{LS}	ΔE_Q [mm s^{-1}]	δ_{iso} [mm s^{-1}]	$\Gamma_{1/2}$ [mm s^{-1}]	γ_{LS}
λ = 820 nm	1.15(8)	1.08*	0.16*	0.14	2.20(20)	1.095*	0.18*	0.03	–	0.445*	0.14*	0.53	–	0.445*	0.14*	0.30
	1.50*		0.22*		–		0.12*									
λ > 780 nm	1.51(2)	1.097(5)	0.17*	0.28	2.35(5)	1.08(1)	0.17*	0.16	–	0.445*	0.156(3)	0.38	–	0.445*	0.155*	0.18
	1.09(1)		0.12*		2.84(2)		0.12*									
λ = 514 nm	0.86(2)	1.071(1)	0.11(2)	0.65	2.67(1)	1.076(2)	0.17*	0.35	–	–	–	–	–	–	–	–
	1.10(2)		0.165(4)		3.00(1)		0.11*									

[a] Asterisks denote fixed parameters. The double-valued parameters ΔE_Q and $\Gamma_{1/2}$ of the HS species are due to the line broadening.

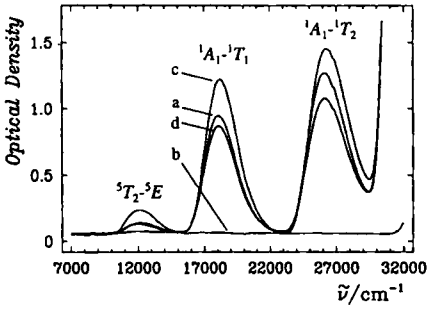

Fig. 12. Unpolarized optical spectra of a single crystal of $[Fe(etz)_6](BF_4)_2$ demonstrating the light-induced spin-crossover processes at 20 K: a) before irradiation, b) after irradiation with λ = 514.5 nm, c) after irradiation with λ = 820 nm, and d) after broad-band irradiation with λ > 780 nm.

3. Discussion

3.1. Thermal Spin-Crossover: The spin transition curves for $[Fe(etz)_6](BF_4)_2$ derived by using various techniques are in agreement with each other. Two thirds of the complexes show a rather steep transition with $T_{1/2}$ = 105 K; one third of the complexes remain in the HS state down to 10 K. Mössbauer spectroscopy identifies the former to be site A complexes and the latter site B. This is quite similar to the behaviour found for $[Fe(mtz)_6](BF_4)_2$ with two crystallographically nonequivalent sites of equal populations. Small differences within the second coordination sphere of the two species stabilize the HS state on site B sufficiently to suppress the spin transition. In addition, there is no evidence for a crystallographic first-order phase transition.

A characteristic feature of $[Fe(etz)_6](BF_4)_2$ is the line broadening within the Mössbauer spectra during the thermal spin transition, which may be due to a distribution of electric hyperfine fields (electric field gradients), at the iron sites. Dynamic processes within the d electron shell, that is LS $\rightleftharpoons$ HS relaxation, may be ruled out. In order to become relevant, the corresponding rate constants would have to be on the order of 10^6–10^7 s^{-1}, which for the R-alkyltetrazole spin-crossover systems is only the case above 170 K.[15] At 100 K, where the broadening becomes large, typical relaxation rate constants for the tetrazole systems are ca. 10 s^{-1}, and they drop to ca. 10^{-4} s^{-1} at 60 K.[16]

Another reason for the distribution of the hyperfine fields could be static or dynamic disorder of the BF_4^- groups. However, in the case of $[Fe(mtz)_6](BF_4)_2$ no comparable line broadening was observed even though the BF_4^- groups are strongly disordered.[5, 6]

Thus, only processes giving rise to a static distribution of hyperfine fields in direct relation to the spin transition need be considered. Owing to the large difference in volume between the HS and LS molecules, there is a build-up of internal pressure or elastic stress during the spin transition. The pronounced layered structure in $[Fe(etz)_6](BF_4)_2$ (Fig. 2) probably reacts very sensitively to shearing forces. For instance, sheets of complexes could be sheared relative to each other if the elastic interactions are anisotropic. Such shear deformations could be transferred via the ethyl substituents of the tetrazole rings to the coordination symmetry of the complex molecules, giving rise to a static distribution of hyperfine fields. In contrast to the internal stress, which builds up during the spin transition and gives rise to anisotropic elastic deformations of the lattice, the application of external pressure acts isotropically on the lattice. In fact, the observation of sharp Mössbauer lines under an external pressure of 1200 bar (Fig. 10) implies a more pronounced long-range order of the crystal lattice under pressure, resulting in a smaller distribution of hyperfine fields for the iron(II) on the two sites. The influence of anisotropic elastic deformations is suppressed upon application of an isotropic external pressure.

A higher degree of order in the crystal lattice provides smaller distributions of zero-point energy differences between the HS and LS states on the two sites, too. Thus one expects a more uniform spin transition behaviour on the two sites. Table 3a and 3b reveal a slightly higher HS(B) concentration at 60 K under 1200 bar ($\approx$37%) than under 1 bar ($\approx$30%). This implies a pressure-induced LS $\rightarrow$ HS conversion of a small proportion of B-site complexes, which, possibly, have undergone a thermal HS $\rightarrow$ LS transition upon cooling at normal pressure (see also Fig. 6). In contrast, the distribution of zero-point energy differences on site A seems to react less sensitively to pressure, since the residual HS(A) fraction at 60 K remains nearly unaffected upon application of pressure. Although this argumentation is rather speculative, we nevertheless believe the shear deformations of the layers in $[Fe(etz)_6](BF_4)_2$ to be the reason for the broadened Mössbauer lines.

3.2. Light-Induced Spin-Crossover: The influence of elastic stress within the crystal lattice during the spin transition is also noticeable after light-induced spin transitions. The different lineshapes of the spectra a–d shown in Figure 11 before and after irradiations indicate different distributions of electric field gradients (EFG), owing to different elastic stresses under the different irradiation conditions. In addition, the inverted intensity ratio of the left- and right-hand lines of the HS(A) doublet between spectra a and b indicates a reorientation of EFG's on site A. This is caused by different elastic stresses before and after LIESST experiments. In order to fully understand this inversion a single-crystal structure determination on the metastable HS state would have to be performed. Whereas the light-induced LS $\rightarrow$ HS conversion is usually quantitative, the HS $\rightarrow$ LS conversion most often does not go to completion. This is due to the

0947-6539/96/0211-1432 $ 15.00+.25/0 Chem. Eur. J. 1996, 2, No. 11

spectral overlap of the $^5T_2-{}^5E$ band of the HS species and the $^1A_1-{}^3T_1$ and $^1A_1-{}^3T_2$ bands of the LS species in the NIR. With reference to Figure 1, the competing intersystem crossing processes lead to a steady-state HS fraction after long irradiation times, which depends upon the degree of spectral overlap at the irradiation wavelengths and the quantum efficiencies of the relevant processes. Thus, irradiation with 514.5 nm, that is, into the $^1A_1-{}^1T_1$ transition of the LS species, results in a quantitative LS(A) → HS(A) conversion, because there is no spectral overlap with any of the transitions characteristic for the HS species (Fig. 11a and 11b).

The nearly complete depopulation of the HS(B) state on irradiation with $\lambda = 820$ nm (Fig. 11c) in $[Fe(etz)_6](BF_4)_2$ allows the immediate conclusion that there is nearly no spectral overlap between the quintet and triplet absorption bands at this wavelength for site B complexes. On the other hand there must be some overlap for A-site complexes at 820 nm, because of the observed steady-state concentration of the HS(A) state.

With broad-band irradiation the same argument holds, except that now the integral spectral overlap has to be considered. Thus broad-band irradiation with $\lambda > 780$ nm covers the full region of the spin-allowed quintet transitions and the spin-forbidden triplet transitions of the LS states for both sites. The ratio of the steady-state HS fractions for the two sites, as derived from the Mössbauer spectrum of Figure 11d, is HS(A):HS(B) = 2:1. This is equal to the ratio of A to B sites in the lattice.

4. Conclusions

This report on the $[Fe(etz)_6](BF_4)_2$ spin-crossover system has completed our studies within the $[Fe(Rtz)_6](BF_4)_2$ series. The $[Fe(etz)_6](BF_4)_2$ system provides a novel combination of structural properties and spin transition features within the $[Fe(Rtz)_6](BF_4)_2$ series. So far, the methyl, ethyl and propyl homologues document a strong interdependence between crystal structure and spin transition, which cannot be predicted based on principle. In $[Fe(etz)_6](BF_4)_2$ there are two nonequivalent lattice sites, which differ drastically in their thermal spin transition behaviour. Site A complexes undergo thermal spin transition; site B complexes remain in the HS(B) state at all temperatures. Nevertheless both sites exhibit light-induced spin transitions. $[Fe(etz)_6](BF_4)_2$ is the first example of a nearly quantitative light-induced HS → LS conversion under irradiation with red light ($\lambda = 820$ nm) for B-site complexes. In addition, the irradiation with green light ($\lambda = 514.5$ nm) leads to the expected quantitative LS → HS conversion on site A. The influence of elastic stress arising during the spin transition has been discussed in terms of a distribution of electric field gradients giving rise to the observed broadening of the Mössbauer lines at temperatures below 105 K. Finally, the possibility of a fine-tuning of the steady-state concentration of the HS fractions under broad-band irradiation has been discussed. The subsequent relaxation processes on the two sites will be described in a further report on $[Fe(etz)_6](BF_4)_2$. This will reveal an unusual aspect of cooperativity—a light-induced bistable spin equilibrium at 70 K.

5. Experimental Procedure

Sample Preparation: The ethyltetrazole ligand was prepared as described in ref. [17]. $[Fe(etz)_6](BF_4)_2$ itself was prepared according to ref. [6]. Single crystals in the form of colourless hexagonal plates of up to several millimeters in diameter and up to 1 mm in thickness were grown from nitromethane by slow evaporation of the solvent in a stream of oxygen-free, dry nitrogen at 295 K.

X-ray Diffraction Measurement: The data collection and refinement parameters are summarized in Table 1. The data were Lorentz and polarization corrected; no absorption correction was applied. The program SIR92 provided the locations of all non-H atoms [18]. 749 parameters were refined by full-matrix least squares, including positional and anisotropic displacement parameters for non-H atoms. The H-atoms were placed in calculated geometric positions and refined with a riding motion model. Atomic scattering factors for all atoms were used as given in SHELXL93 [19]. Final refinement converged to $R = 0.103$ ($wR2 = 0.373$). The BF_4^- groups are strongly disordered. The structure plots were provided by the programs SCHAKAL92 and PLUTO76 [20,21]. Further details of the crystal structure investigations may be obtained from the Fachinformationszentrum Karlsruhe, 76344 Eggenstein-Leopoldshafen (Germany) on quoting the depository number CSD-380096.

^{57}Fe Mössbauer Spectroscopy: Mössbauer spectra were recorded in transmission geometry with a Co/Rh source kept at room temperature and a conventional spectrometer operating in the constant-acceleration mode. The samples were sealed in polished Plexiglass containers (3 cm^2; ≈4 mg Fe per cm^2) and mounted in a helium-flow cryostat (CF506, Oxford Instruments). The cryostat was equipped with windows of transparent Mylar foils for irradiation experiments. The temperature was measured with a carbon/glass resistor, mounted directly on the sample holder to control the temperature during irradiation. The spectra were fitted to Lorentzians with the program MOSFUN [22], assuming equal Debye–Waller factors for the HS and LS states at a given temperature.

Magnetic Susceptibility: Magnetic susceptibilities were measured with a FONER-type magnetometer (Princeton Applied Research), equipped with a helium-flow cryostat (Cryovac), in an external field of 1 T between 25 and 293 K. Effective magnetic moments were calculated from $\mu_{eff} = \sqrt{8\chi T}$, where χ is the corrected molar susceptibility. The diamagnetic correction of $[Fe(etz)_6](BF_4)_2$ was calculated from Pascal's constants ($\chi_{dia} \approx -400 \times 10^{-6}$ cm^3 mol^{-1}). With the assumption of a simple Curie law behaviour for the HS state and a temperature-independent susceptibility for the LS state, the HS fraction γ_{HS} may be calculated from the experimentally determined susceptibilities.

Optical Spectroscopy: Single-crystal absorption spectra were recorded with a UV/Vis/NIR spectrometer (Bruins Instruments, Omega-10). All spectra could be measured unpolarized, because of negligibly small polarization effects. Sample temperatures down to 10 K were achieved with a technique using a cold helium gas flow tube [23]. The temperature was measured with a calibrated gold–iron/chromel thermocouple, a fraction of a millimeter away from the crystal. The reference junction was kept in liquid nitrogen. The spectra as shown here were obtained after subtracting a baseline from all measured data.

Pressure Experiments: The experiments were performed with a conventional Mössbauer spectrometer in combination with a special compressor system. The compressor provides pressures up to 1200 bar by compression of helium gas within a gas-tight cell. The sample was mounted inside this cell, which was equipped with windows of boron carbide. These were transparent to the γ-rays, but contained an iron(III) impurity. The subspectrum of the impurity was subtracted from the collected data.

Irradiation Experiments: Narrow-band irradiation experiments were performed with an argon laser (Spectra Physics 2020) at 514.5 nm and with a Ti–sapphire laser (Spectra Physics 3900) at 820 nm. Laser powers used were of the order of a few tens of milliwatts with irradiation times of a few minutes. For broad-band irradiation experiments, a Xe arc lamp (Type XBO150W/1) was used in combination with cut-off filters RG570, RG590, RG610, RG695 and RG780 (Schott), transparent to $\lambda > 570$, 590, 610, 695 and 780 nm, respectively.

Acknowledgement: This work was financially supported by the Deutsche Forschungsgemeinschaft, the Fonds der Chemischen Industrie, the Schweizerische National Fonds, the Materialwissenschaftliches Forschungszentrum der Universität Mainz and the European Community (Network Contract No. ERBCHRX CT920080). We thank U. Stumm and P. Dickmann for assisting in the ^{57}Fe Mössbauer experiments under pressure.

Received: March 15, 1996 [F322]

[1] J. K. Beattie in *Advances in Inorganic Chemistry* (Ed.: A. G. Sykes), Academic Press, San Diego, California, **1988**, *32*, pp. 1–53.
[2] H. Toftlund, *Coord. Chem. Rev.* **1989**, *94*, 67–108.
[3] E. König, *Struct. Bonding* **1991**, *76*, 51–152.
[4] P. Gütlich, A. Hauser, H. Spiering, *Angew. Chem.* **1994**, *106*, 2109–2141; *Angew. Chem. Int. Ed. Engl.* **1994**, *33*, 2024–2054.
[5] L. Wiehl, *Acta Crystallogr. Sect. B* **1993**, *49*, 289–303.
[6] P. Poganiuch, S. Decurtins, P. Gütlich, *J. Am. Chem. Soc.* **1990**, *112*, 3270–3278.
[7] A. Ozarowski, B. R. McGarvey, *Inorg. Chem.* **1989**, *28*, 2262–2266.

[8] S. Decurtins, P. Gütlich, C. P. Köhler, H. Spiering, A. Hauser, *Chem. Phys. Lett.* **1984**, *105*, 1–4.
[9] S. Decurtins, P. Gütlich, K. M. Hasselbach, A. Hauser, H. Spiering, *Inorg. Chem.* **1985**, *24*, 2174–2178.
[10] A. Hauser, *J. Chem. Phys.* **1991**, *94*, 2741–2748.
[11] A. Hauser, P. Gütlich, H. Spiering, *Inorg. Chem.* **1986**, *25*, 4245–4248.
[12] A. Hauser, *Chem. Phys. Lett.* **1986**, *124*, 543–548.
[13] R. Hinek, P. Gütlich, A. Hauser, *Inorg. Chem.* **1994**, *33*, 567–572.
[14] A. B. P. Lever, *Inorganic Electronic Spectroscopy*, Elsevier, Amsterdam, **1984**, p. 462.
[15] P. Adler, H. Spiering, P. Gütlich, *Hyperfine Interact.* **1989**, *52*, 47–63.
[16] A. Hauser, A. Vef, P. Adler, *J. Chem. Phys.* **1991**, *95*, 8710–8717.
[17] P. L. Franke, J. G. Haasnoot, A. P. Zuur, *Inorg. Chim. Acta* **1982**, *59*, 5–9.
[18] A. Altomare, C. Giacovazzo, G. Cascarano, A. Guagliardi, *J. Appl. Crystallogr.* **1994**, *27*, 435.
[19] G. M. Sheldrick, *SHELXL93—Program for Crystal Structure Refinement*, Univ. of Göttingen, Germany.
[20] E. Keller, *SCHAKAL92. A Computer Program for the Graphic Representation of Molecular and Crystallographic Models*, Univ. of Freiburg, Germany.
[21] S. Motherwell, B. Clegg, *PLUTO76. Program for Plotting the Molecular and Crystal Structures*, Univ. of Cambridge, England.
[22] E. W. Müller, *Ph.D. Thesis*, **1982**, Univ. of Mainz, Germany.
[23] E. R. Krausz, *J. Phys. Sect. E*, **1982**, *15*, 1167–1168.

0947-6539/96/0211-1434 $ 15.00+.25/0 *Chem. Eur. J.* **1996**, *2*, *No. 11*